

Saturation of vibrational coherent anti-Stokes Raman scattering mediated by saturation of the rotational Raman transition

Anil K. Patnaik,^{1,2,*} Sukesh Roy,³ and James R. Gord¹

¹*Air Force Research Laboratory, Aerospace Systems Directorate, Wright-Patterson AFB, Ohio 45433, USA*

²*Department of Physics, Wright State University, Dayton, Ohio 45435, USA*

³*Spectral Energies, LLC, 5100 Springfield Street, Suite 301, Dayton, Ohio 45431, USA*

(Received 5 December 2012; published 2 April 2013)

Saturation of vibrational Raman coherence and coherent anti-Stokes Raman scattering (CARS) using femtosecond (fs) excitation pulses is investigated theoretically. The pump in a typical fs-CARS configuration has a bandwidth of a few hundred cm^{-1} that can couple *tens of rotational states* of room-air nitrogen molecules simultaneously, unlike in CARS with longer pulse durations. It is demonstrated that the vibrational coherence and also the vibrational CARS with fs excitation display saturationlike behavior once the rotational coherence is saturated. The Raman saturation threshold for the fs pump is numerically estimated to be at a peak intensity of $\sim 10^{22}$ W/m^2 , which is six to seven orders of magnitude higher than that in the nanosecond regime. The results are compared with the known saturation thresholds in different pulse-duration regimes and placed in perspective with other nonlinear thresholds reported in fs excitation regimes.

DOI: [10.1103/PhysRevA.87.043801](https://doi.org/10.1103/PhysRevA.87.043801)

PACS number(s): 42.65.Dr, 82.53.Kp

I. INTRODUCTION

The accuracy of spectroscopy in any linear or nonlinear optical technique relies on the fact that there are regimes of linear dependencies on the excitation [1]. For example, in typical continuous-wave (cw) coherent anti-Stokes Raman scattering (CARS), where two lasers with pump intensity I_p and Stokes intensity I_s generate the Raman coherence and the probe with intensity I_{pr} beats with the coherence to generate the CARS signal [2],

$$I_{\text{CARS}} \propto I_p I_s I_{pr}. \quad (1)$$

The CARS signal grows with an increase in any one of the intensities I_α ($\alpha \rightarrow p, s, pr$)—but with certain limits. Since the maximum achievable Raman coherence is only 0.5, depending on the strength of the couplings, there exists a limit for the product $I_p I_s$ beyond which the CARS signal will saturate. If the laser intensities are increased further, the Raman transitions will experience a Stark shift [3]; hence, the spectral shape of the CARS signal will become distorted [4–7]. Similar conclusions have been drawn concerning the saturation in other four-wave-mixing-based spectroscopic techniques in the nanosecond (ns) and picosecond (ps) excitation regimes [8–11]. A strong probe could also saturate the CARS signal—in particular, in electronic-resonant-enhanced CARS configurations [12–14].

In the femtosecond (fs) CARS technique, however, the above description of Raman coherence is further complicated by the fact that a fs pulse is associated with a large bandwidth, e.g., a 100-fs pulse at 532 nm has a bandwidth of ~ 350 cm^{-1} , which can couple to multiple molecular states simultaneously; e.g., the rotational-frequency separation in the ground vibrational state of nitrogen is ~ 8 cm^{-1} . A schematic of the N_2 molecule with fs lasers in a CARS configuration is depicted in Fig. 1. Clearly, the pump alone has sufficient bandwidth to create coherences among the multiple rotational levels, unlike

in ns or ps excitations. Note that multiple pumps have been used to realize simultaneous rotational and vibrational CARS in the ns excitation regime [15]. Since the cross section of the rotational Raman process is at least an order of magnitude higher than that of the vibrational Raman process [2], the rotational Raman coherence ρ_{rot} generated by the pump alone might saturate with a lower pump intensity than the vibrational coherence ρ_{vib} . It is, therefore, important to study how the rotational coherence generated by the broad bandwidth of the pump affects the vibrational coherence and, hence, the CARS signal. In this paper, we address the above issue and also estimate the saturation limit in this fs CARS system. We compare the limiting value with other nonlinear thresholds in the fs excitation regime and also with other long-pulse regimes.

Recently, fs CARS has been the subject of intense interest among gas-phase spectroscopy researchers [16], especially since Silberberg and co-workers demonstrated that pulses with bandwidth larger than the linewidth of the atomic or molecular levels under interrogation can be used to advantage—in particular, in multiphoton interactions [17]. Other advantages of fs CARS for practical applications include the ability to take high-speed single-shot snapshots with high-repetition-rate lasers from 1 to 10 kHz [18,19], collision-free spectroscopy for pressures up to 50 bars [20,21], and the potential to perform CARS with a single beam [22,23]. Time-resolved fs CARS measurements have been used extensively for temperature and concentration measurements in our group [16,24]. However, with the availability of new high-power fs lasers, the physics of saturation via broadband coupling has become extremely important for understanding the scope and limitations of the fs-CARS-based diagnostic.

In Sec. II, we consider a simplified model and describe its dynamics using the density-matrix equations. We present numerical solutions and discuss the results for the saturation of rotational and vibrational Raman coherence and, hence, for the CARS signal in Sec. III. In Sec. IV, we compare our results with the known saturation thresholds in different pulse-duration regimes and place our results in perspective with

*anil.patnaik@wpafb.af.mil

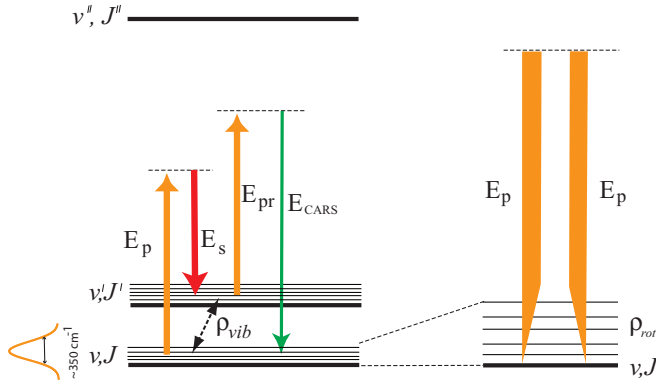


FIG. 1. (Color online) The wide bandwidth associated with the pump field E_p (pulse duration of 100 fs) couples the rotational states within the same vibrational manifold, creating a strong rotational coherence in addition to its role of pump for the vibrational CARS configuration. The Stokes, probe, and generated CARS fields are represented by E_s , E_{pr} , and E_{CARS} , respectively. The ground (excited) vibrational manifold in the ground (excited) electronic state is v (v'), with the rotational states being represented by J (J'). The vibrational (rotational) states in the excited electronic state are represented by v'' (J''). Rotational (vibrational) coherences are denoted by ρ_{rot} (ρ_{vib}).

other nonlinear thresholds reported in fs excitation regimes. We summarize the results in Sec. V.

II. THE MODEL AND CALCULATION OF CARS POLARIZATION

As mentioned earlier, the fs CARS system presented in Fig. 1 involves simultaneous Raman coupling of multiple rotational levels J and J' in each of the vibrational levels v and v' , respectively, in the ground electronic state that satisfy the Raman resonance condition. Since our specific goal is to examine the effect of saturation of the rotational Raman excitations on the vibrational coherence—and, hence, CARS signal—we consider a simplified four-level model system as shown in Fig. 2. Our system consists of two rotational levels ($|n_1\rangle, |n_2\rangle$) in their ground vibrational state ($v = 0$), one rotational level $|m\rangle$ in the first excited vibrational state ($v = 1$), and an excited level $|e\rangle$ that is representative of

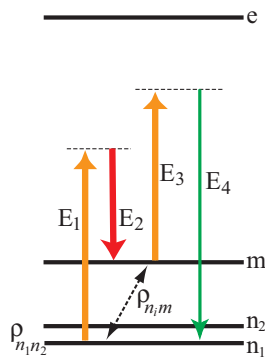


FIG. 2. (Color online) Model scheme where the broad bandwidth associated with the pump field E_1 couples two rotational states n_1 and n_2 , creating a rotational coherence $\rho_{n_1n_2}$. The pump and Stokes fields E_1 and E_2 generate the vibrational coherences ρ_{n_1m} that are directly affected by the rotational coherence $\rho_{n_1n_2}$.

all the excited electronic states. A single fs pump field E_1 couples the two rotational states $|n_1\rangle$ and $|n_2\rangle$ to generate the coherence between them. The Stokes field E_2 couples those states to the rovibrational state $|m\rangle$ (corresponding to $v = 1$) and generates the vibrational coherences between the states $|n_i\rangle$ and $|m\rangle$ ($i = 1, 2$). The vibrational coherences are then scattered by the probe field E_3 to produce the CARS signal E_4 . All of the parameters used in the calculations are considered to be close to their values for the N_2 molecule, except for the total number of rotational levels involved in the interaction. At room temperature the states $|n_1\rangle$ and $|n_2\rangle$ could correspond to $J = 8$ and 10 , respectively, that contain the maximum population compared to the other J states in the $v = 0$ vibrational manifold of the electronic state. The state $|m\rangle$ could correspond to $J = 8$ of $v = 1$ so that the Q - and O -branch rovibrational Raman lines would be excited by coupling of the fields E_1 and E_2 .

The three input pulses considered here are Gaussian pulses $\vec{E}_i(t)$, $i \rightarrow 1$ to 3; thus, the total field is given by

$$\vec{E}(t) = \sum_i \hat{e}_i |E_{i0}| e^{-(t-t_i)^2/\tau_i^2} e^{-iv_it} + \text{c.c.} \quad (2)$$

Here, \hat{e}_i , t_i , τ_i , and v_i are the polarization, the peak position of the pulse, the duration of the pulse, and the central frequencies of the applied fields, respectively. For simplicity, we consider polarizations of all three fields to be linear and parallel to each other. The interaction of these pulses with the molecule is given by the interaction Hamiltonian in the dipole approximation as [25]

$$\begin{aligned} H_I &= -\vec{\phi} \cdot \vec{E}(t) \\ &= -\hbar\Omega_1(t)e^{-iv_1t} (|e\rangle\langle n_1| + |e\rangle\langle n_2|) \\ &\quad -\hbar[\Omega_2(t)e^{-iv_2t} + \Omega_3(t)e^{-iv_3t}]|e\rangle\langle m| + \text{H.c.} \end{aligned} \quad (3)$$

Here, $\vec{\phi}$ is the induced molecular dipole moment. Note that in writing the above equation, the following approximations are made: (1) the spatial dependence of the pulses during propagation is ignored, assuming point interaction with a single molecule or interaction with an optically thin medium, (2) the electric field \vec{E}_i and the corresponding transition dipole moments are assumed to be parallel, and (3) the antiresonant terms such as $\Omega_i(t)e^{-iv_it}|n_i\rangle\langle e|$ have been eliminated from H_I using the rotating-wave approximation [25]. The Rabi frequencies corresponding to coupling between the molecule and the laser pulses are

$$\Omega_1 = \frac{\wp_{en_i}|E_{10}|}{\hbar} \quad \text{and} \quad \Omega_\alpha = \frac{\wp_{em}|E_{\alpha 0}|}{\hbar}, \quad (4)$$

where $\alpha = 2, 3$ and $i = 1, 2$. Here the transition matrix elements are given by [26]

$$\begin{aligned} \wp_{en_1} &= \wp_{en_2} = \langle e|q_e r|n_i\rangle F_{v_e v_n} R_{J_e J_{n_i}}, \\ \wp_{em} &= \langle e|q_e r|m\rangle F_{v_e v_m} R_{J_e J_m}. \end{aligned} \quad (5)$$

Note that the dipole moments corresponding to both rotational transitions are assumed to be approximately the same. The numerical value of the dipole moment $\langle q_e r \rangle$ is determined to be $\sim 1.2 \times 10^{-33}$ C m from the spontaneous decay rate of the excited electronic state $A^3 \Sigma_u^+$ [27]. Here, q_e is the charge of the electron and r is the dipole separation; $F_{v_e v_n} = \langle v_e | v_n \rangle$

($F_{v_e v_m} = \langle v_e | v_m \rangle$) are the Frank-Condon (FC) factors that determine the overlap between the ground (excited) vibrational states of the ground electronic state and all of the vibrational states in the excited electronic states. In particular, since the state $|e\rangle$ is only a representative state of *all* of the excited states that may have significant overlapping integral contributions to the FC factor, the vibrational state $|v_e\rangle$ associated with $|e\rangle$ is not a single vibrational state; rather it is a linear combination of all the vibrational states in that electronic state, i.e., $|v_e\rangle \equiv \sum_j |v_{e_j}\rangle$. Note that for the purpose of the current calculations, we have used the equilibrium values of the FC parameters of N_2 [28] to calculate the Rabi frequencies. The rotational overlap functions are denoted by $R_{J_e J_{n_i}}$ and $R_{J_e J_m}$.

The unperturbed Hamiltonian of the model system is given by

$$H_0 \equiv \hbar \left[\omega_e |e\rangle \langle e| + \omega_m |m\rangle \langle m| + \sum_{i=1,2} \omega_{n_i} |n_i\rangle \langle n_i| \right]. \quad (6)$$

Here, $\hbar\omega_\alpha$ is the unperturbed energy of the molecular state $|\alpha\rangle$ in the model ($\alpha \rightarrow n_i, m, \text{ and } e$). The time-resolved dynamics of the molecular polarization can, thus, be obtained by deriving the density-matrix equations of motion for the molecule-laser-coupled system as

$$\frac{\partial \rho}{\partial t} = -\frac{i}{\hbar} [H_0 + H_I, \rho] + \text{decay parameters}. \quad (7)$$

Note that the decay parameters are introduced phenomenologically and are discussed in detail later.

To derive the density-matrix equation, we substitute H_0 and H_I from Eqs. (6) and (3) and write the equations for the individual density-matrix elements. The dynamical equations are associated with fast-oscillating terms that oscillate at laser frequencies of $\pm v_i$ ($i \rightarrow 1, 2, 3$). To remove such oscillations, we use the following rotations to separate the polarizations that are oscillating at different frequencies [29]:

$$\begin{aligned} \rho_{en_i} &= \sigma_{en_i} e^{-iv_1 t} + \eta_{en_i} e^{-iv_4 t}, \\ \rho_{em} &= \sigma_{em} e^{-iv_2 t} + \eta_{em} e^{-iv_3 t}, \\ \rho_{n_i m} &= \tilde{\rho}_{n_i m} e^{-i(v_1 - v_2)t}. \end{aligned} \quad (8)$$

Here, $\rho_{\alpha\beta}$ are the coherence-matrix elements between the levels $|\alpha\rangle$ and $|\beta\rangle$; $\sigma_{\alpha\beta}$, $\eta_{\alpha\beta}$, and $\tilde{\rho}_{\alpha\beta}$ are the transformed coherence-density-matrix elements that oscillate at particular frequencies determined by above transformations. The transformations (8) also allow us to separate the molecular polarizations within the same transitions that are oscillating at different frequencies. For example, we know that the CARS signal will be generated at around $v_4 = v_3 - (v_1 - v_2)$; therefore, in anticipation of the CARS polarization, we have introduced the density-matrix element η_{en_i} that oscillates at around v_4 . Using these transformations, the density-matrix equations for the model system are obtained as follows. For clarity, we have grouped the equations according to the nature of the coherence-density-matrix elements. The evolution of the rotational Raman coherence is given by

$$\begin{aligned} \frac{\partial \rho_{n_1 n_2}}{\partial t} &= -(\gamma_{n_1 n_2} + i\omega_{n_1 n_2}) \rho_{n_1 n_2} \\ &\quad - i[\Omega_1 \sigma_{n_1 e} + \Omega_1 \eta_{n_1 e} e^{-i(\Delta_2 - \Delta_1)t}] \\ &\quad + i[\Omega_1^* \sigma_{en_2} + \Omega_1^* \eta_{en_2} e^{i(\Delta_2 - \Delta_1)t}]. \end{aligned} \quad (9)$$

The evolution of the vibrational Raman coherences is given by

$$\begin{aligned} \frac{\partial \rho_{n_1 m}}{\partial t} &= -\gamma_{n_1 m} \rho_{n_1 m} - i[\Omega_2 \sigma_{n_1 e} + \Omega_3 \eta_{n_1 e} \\ &\quad + \Omega_2 \eta_{n_1 e} e^{-i(\Delta_2 - \Delta_1)t} + \Omega_3 \sigma_{n_1 e} e^{i(\Delta_2 - \Delta_1)t}] \\ &\quad + i[\Omega_1^* \sigma_{em} + \Omega_1^* \eta_{em} e^{i(\Delta_2 - \Delta_1)t}], \end{aligned} \quad (10)$$

$$\begin{aligned} \frac{\partial \rho_{n_2 m}}{\partial t} &= -(\gamma_{n_2 m} + i\omega_{n_2 n_1}) \rho_{n_2 m} - i[\Omega_2 \sigma_{n_2 e} + \Omega_3 \eta_{n_2 e} \\ &\quad + \Omega_2 \eta_{n_2 e} e^{-i(\Delta_2 - \Delta_1)t} + \Omega_3 \sigma_{n_2 e} e^{i(\Delta_2 - \Delta_1)t}] \\ &\quad + i[\Omega_1^* \sigma_{em} + \Omega_1^* \eta_{em} e^{i(\Delta_2 - \Delta_1)t}]. \end{aligned} \quad (11)$$

Note that the tildes in $\tilde{\rho}_{n_i m}$ are dropped for brevity. The coherence terms involving the excited electronic state are

$$\begin{aligned} \frac{\partial \sigma_{n_1 e}}{\partial t} &= -(\gamma_{n_1 e} - i\Delta_1) \sigma_{n_1 e} + i\Omega_1^* (\rho_{ee} - \rho_{n_1 n_1}) \\ &\quad - i\Omega_1^* \rho_{n_1 n_2} - i\Omega_2^* \rho_{n_1 m}, \end{aligned} \quad (12)$$

$$\begin{aligned} \frac{\partial \sigma_{n_2 e}}{\partial t} &= -[\gamma_{n_2 e} + i(\omega_{n_2 n_1} - \Delta_1)] \sigma_{n_2 e} + i\Omega_1^* (\rho_{ee} - \rho_{n_2 n_2}) \\ &\quad - i\Omega_1^* \rho_{n_2 n_1} - i\Omega_2^* \rho_{n_2 m}, \end{aligned} \quad (13)$$

$$\frac{\partial \eta_{n_1 e}}{\partial t} = -(\gamma_{n_1 e} - i\Delta_2) \sigma_{n_1 e} - i\Omega_3^* \rho_{n_1 m}, \quad (14)$$

$$\frac{\partial \eta_{n_2 e}}{\partial t} = -[\gamma_{n_2 e} + i(\omega_{n_2 n_1} - \Delta_2)] \eta_{n_2 e} - i\Omega_3^* \rho_{n_2 m}, \quad (15)$$

$$\begin{aligned} \frac{\partial \sigma_{me}}{\partial t} &= -(\gamma_{me} - i\Delta_1) \sigma_{me} + i\Omega_2^* (\rho_{ee} - \rho_{mm}) \\ &\quad - i\Omega_1^* (\rho_{mn_1} + \rho_{mn_2}), \end{aligned} \quad (16)$$

$$\frac{\partial \eta_{me}}{\partial t} = -(\gamma_{me} - i\Delta_2) \eta_{me} + i\Omega_3^* (\rho_{ee} - \rho_{mm}). \quad (17)$$

Here, the matrix elements $\rho_{\alpha\alpha}$ represent the populations in the state $|\alpha\rangle$; $\Delta_1 = \omega_{en_1} - v_1 = \omega_{em} - v_2$ ($\Delta_2 = \omega_{em} - v_3$) is the frequency detuning of the pump or Stokes (probe) field from the electronic transition.

All of the decay and dephasing parameters $\gamma_{\alpha\beta}$ are introduced phenomenologically. For calculation purposes we assume an open-system approach for the decay parameters of the molecular states. We now present a brief account of the the different phenomenological decay and dephasing parameters used in the model calculation.

(a) *Spontaneous emission.* Since the natural decay lifetime of the excited state of N_2 is very long (on the order of seconds), we have ignored it in the dynamical equations where the time scales of concern are on the order of tens of picoseconds. However, it should be noted that the spontaneous decay determines the induced-dipole matrix element that is crucial for determining the strength of the laser-molecule Rabi couplings (4) in the interaction Hamiltonian Eq. (3).

(b) *Vibrational-energy transfer rate.* The vibrational-energy transfer (VET) or the transfer of population among the vibrational states of the N_2 molecule within its ground electronic state as a result of collisions occurs at a rate of $\Gamma_{\text{VET}} \sim 10^6 \text{ s}^{-1}$ at atmospheric pressure and room temperature [30].

(c) *Rotational-energy transfer rate.* The rotational states transfer population among themselves within the same vibrational manifold because of inelastic collisions; such

rotational-energy transfer (RET) rates for N_2 are typically $\Gamma_{\text{RET}} \sim 2.7 \times 10^{10} \text{ s}^{-1}$ at room temperature [31].

(d) *Pure dephasing rate.* The rate of pure dephasing (PD) of coherence in N_2 in elastic collisions is twice the RET rate; i.e., $\gamma^{PD} \sim 2\Gamma_{\text{RET}}$ [32]. For calculation purposes, assuming that the RET, VET, and pure dephasing rates are of same order in the excited electronic state $|e\rangle$, the decay rates γ_{ij} used in Eqs. (9)–(17) are $\gamma_{ij} = -(\Gamma_{\text{RET}} + \Gamma_{\text{VET}} + \gamma^{PD})$.

The instantaneous macroscopic polarization may be written [25] in terms of the density matrix as $\vec{P}(t) = N\text{Tr}[\rho(t)\vec{\rho}]$; here, N is the number density of the molecules in the probe volume, $\text{Tr}[\]$ is the trace of the matrix in brackets, and $\vec{\rho}$ is the dipole moment corresponding to the transition for which the molecular polarization is being calculated. The CARS signal intensity that is observed in the laboratory is proportional to the square of the third-order molecular polarization $P^{(3)}$. The time-resolved CARS signal is calculated as [29]

$$I_{\text{CARS}}(t) \sim \int_{-\infty}^t |P^{(3)}(t')|^2 dt'. \quad (18)$$

For our model system the third-order polarizations or the molecular polarizations oscillating at CARS frequencies are η_{n_1e} and η_{n_2e} . Thus, the time-resolved CARS signal for our model can be written as

$$I_{\text{CARS}}(t) \sim \int_{-\infty}^t |\eta_{n_1e}(t') + \eta_{n_2e}(t')|^2 dt', \quad (19)$$

with the arbitrariness of a proportionality constant.

In the following section we present the numerical solutions to the above coupled density-matrix equations (9)–(17) for obtaining the rotational coherence $\rho_{n_1n_2}$ and vibrational coherence ρ_{n_1m} and the CARS signal I_{CARS} to study the saturation effects.

III. NUMERICAL RESULTS: SATURATION OF RAMAN COHERENCES AND CARS

The coupled equations (9)–(17) derived in the previous section completely describe the dynamics of the model system under consideration. Those equations are solved numerically using the fifth-order Runge-Kutta method, and the results are presented for both coherences and also the CARS polarizations for different parametric conditions to aid the understanding of the effect of saturation of the rotational states. All of the plots presented in this paper are generated from these full numerical solutions of the density-matrix equations. We also present the approximate analytical equations to provide a clearer understanding wherever possible. In the Sec. III A, we discuss how the rotational and vibrational coherences are saturated by increasing the pump intensity; in Sec. III B, we present results showing how saturation affects the rovibrational CARS signal.

A. Saturation of Raman coherences

As noted earlier the broad bandwidth associated with the fs pump couples both the rotational lines in the ground vibrational states; the primary goal of this study is to examine how saturation of such rotational lines affects other dynamics, such as the vibrational coherence and the CARS signal.

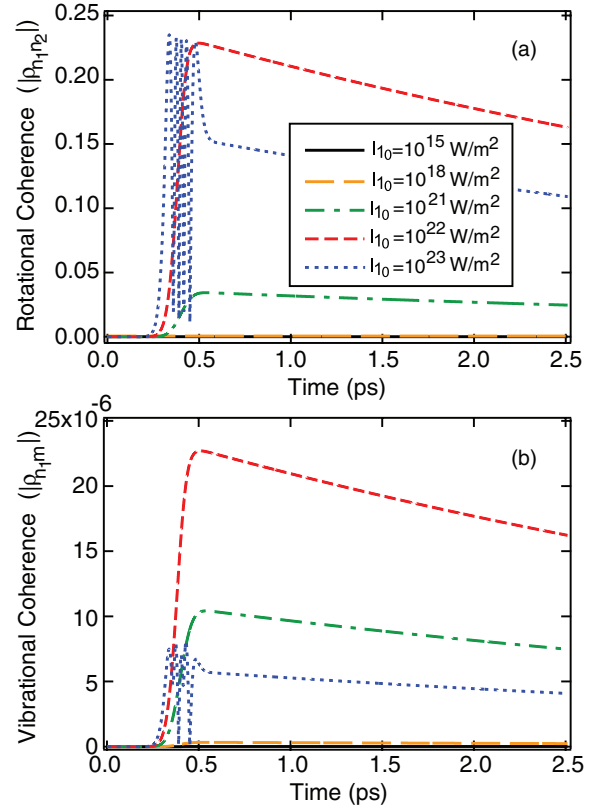


FIG. 3. (Color online) (a) Dynamics of rotational coherence. Saturation of rotational coherence is observed with increased peak intensity of the pump. (b) The corresponding saturation observed in vibrational coherence.

Hence, we parametrically changed the peak intensity of the pump, starting from its operational value of $\sim 10^{15} \text{ W/m}^2$, which our group employed [33] to study the magnitude of the rotational coherence $|\rho_{n_1n_2}|$ and vibrational coherence $|\rho_{n_1m}|$, as shown in Fig. 3. The parameters considered here are as follows: The pulse duration of both pump (τ_1) and Stokes (τ_2) pulses is $\sim 100 \text{ fs}$ and both appear at $\sim 400 \text{ fs}$. The central frequency of the pump (Stokes) is $\sim 675 \text{ nm}$ ($\sim 800 \text{ nm}$). Here, the peak intensity of the Stokes pulse is maintained at $I_{20} \sim 4 \times 10^{15} \text{ W/m}^2$ [33], and the pump intensity I_{10} is varied parametrically to determine the limit at which saturation appears. For the purpose of the current calculation, we considered the initial population in the states $|n_1\rangle$ and $|n_2\rangle$ to be 0.75 and 0.25, respectively.

In Fig. 3(a), the rotational coherence $|\rho_{n_1n_2}(t)|$ is presented for different values of the peak intensities of the pump, starting from $\sim 10^{15} \text{ W/m}^2$. For each value of the peak intensity of the pump $I_{10} \leq 10^{22} \text{ W/m}^2$, the rotational coherence exhibits a monotonic increase on the rising side of the pump and Stokes pulses; on the falling side the coherence value $|\rho_{n_1n_2}(t)|$ achieves a certain quasi-steady-state value for our period of observation of $\sim 2.5 \text{ ps}$. The slow decay during the 2.5 ps occurs primarily because of γ^{PD} and Γ_{RET} . The maximum value of $|\rho_{n_1n_2}|$ and the corresponding quasi-steady-state values increase up to ~ 0.25 (near the allowed maximum value of 0.5) with the pump intensities until the coherence is saturated at $I_{10} > 10^{22} \text{ W/m}^2$. For $I_{10} > 10^{23} \text{ W/m}^2$, Rabi oscillations

appear in $|\rho_{n_1n_2}(t)|$, where a few cycles of coherence oscillation appear within the pulse duration of 100 fs before the coherence achieves a quasi-steady-state value of $|\rho_{n_1n_2}| \sim 0.1$.

In Fig. 3(b), we present the corresponding plots for the vibrational coherence $|\rho_{n_1m}(t)|$. All of the parameters and legends are the same as in Fig. 3(a) to facilitate comparison. Once again, corresponding to each value of the pump intensity, $|\rho_{n_1m}(t)|$ is associated with a monotonic increase on the rising side of the pump and Stokes pulses, which later reaches a quasi-steady-state value after achieving the maximum value. Interestingly, for $I_{10} > 10^{22}$ W/m², where the rotational coherence is saturated, the vibrational coherence also exhibits saturationlike behavior. However, the maximum value of $|\rho_{n_1m}| \approx 2.3 \times 10^{-5}$ for $I_{10} = 10^{22}$ W/m² is still far from the maximum achievable coherence of 0.5. Clearly, the saturationlike behavior thereof is due to the saturation in the rotational states. A Rabi oscillation in the vibrational coherence is also observed for $I_{10} = 10^{23}$ W/m². Furthermore, the corresponding quasi-steady-state value is less than that obtained by a two-orders-of-magnitude lower pump peak intensity.

To examine the role of rotational coherence in the dynamics of vibrational coherence and achieve further analytical understanding of saturation, we carried out the following approximate calculation: Assuming that the single-photon detunings $\Delta_1 \gg \Omega_1, \Omega_2, \gamma^{PD}$, and Γ_i , it may also be assumed that the excited state is never populated, i.e., $\rho_{ee} = 0$. Thus, in the absence of the probe field $E_3 = 0$ and ignoring all of the decay and dephasing parameters, the dynamical equation for the rotational coherence reduces to

$$\begin{aligned} \frac{\partial \rho_{n_1n_2}}{\partial t} = & -i \left(\omega_{n_2n_1} + \frac{|\Omega_1|^2}{\Delta_1} - \frac{|\Omega_1|^2}{\Delta_1 + \omega_{n_2n_1}} \right) \rho_{n_1n_2} \\ & + i \frac{|\Omega_1|^2}{\Delta_1} \left(\frac{\Delta_1}{\Delta_1 + \omega_{n_2n_1}} \rho_{n_2n_2} - \rho_{n_1n_1} \right) \\ & - i \frac{\Omega_1^* \Omega_2^*}{\Delta_1} \rho_{n_1m} + i \frac{\Omega_1^* \Omega_2}{\Delta_1 + \omega_{n_2n_1}} \rho_{mn_2}, \end{aligned} \quad (20)$$

and that for the vibrational coherence ρ_{n_1m} reduces to

$$\begin{aligned} \frac{\partial \rho_{n_1m}}{\partial t} = & -i \frac{\Omega_1^* \Omega_2}{\Delta_1} \rho_{n_1n_2} + i \frac{\Omega_1^* \Omega_2}{\Delta_1} (\rho_{mm} - \rho_{n_1n_1}) \\ & + \frac{i}{\Delta_1} (|\Omega_2|^2 - |\Omega_1|^2) \rho_{n_1m} + i \frac{|\Omega_1|^2}{\Delta_1} \rho_{n_2m}. \end{aligned} \quad (21)$$

It is clear that $\Delta_1 \gg \omega_{n_1n_2}$; also, at near saturation we know that the intensity of the pump pulse is orders of magnitude larger than that of the Stokes pulse, and hence $|\Omega_1|^2 \gg |\Omega_2|^2$. Thus, with these approximations, we can rewrite the above equations for near-saturation conditions as

$$\begin{aligned} \frac{\partial \rho_{n_1n_2}}{\partial t} & \approx i \frac{|\Omega_1|^2}{\Delta_1} (\rho_{n_2n_2} - \rho_{n_1n_1}), \quad (22) \\ \frac{\partial \rho_{n_1m}}{\partial t} & \approx -i \frac{\Omega_1^* \Omega_2}{\Delta_1} (\rho_{n_1n_1} - \rho_{mm} + \rho_{n_1n_2}) \\ & + i \frac{|\Omega_1|^2}{\Delta_1} (\rho_{n_2m} - \rho_{n_1m}). \quad (23) \end{aligned}$$

Several interesting conclusions can be drawn from the above approximate equations of the coherence matrix elements: (1) Since we have eliminated the decay and dephasing terms to obtain the above equations, we cannot deduce the

conditions for saturation directly from the them. However, the near-saturation behavior can be understood extremely well from Eqs. (22) and (23). The Rabi oscillations that appear in $|\rho_{n_1n_2}(t)|$ in Fig. 3(a) at near-saturation conditions are due to the rotational two-photon Rabi coupling $|\Omega_1|^2/\Delta_1 = \Omega_{2\text{ph}}^R$ in Eq. (22), which is equivalent to an isolated, driven two-level system. (2) In a hypothetical case involving the absence of the broadband coupling of the two rotational states by the fs pump, the rotational coherence would never evolve, i.e., the right-hand side of Eq. (22) would be zero. And in Eq. (23), the first term in the parentheses with the rotational coherence $\rho_{n_1n_2}$ would be absent. Also, the second interfering term that involves $\Omega_{2\text{ph}}^R$ would become zero. In such a case the vibrational coherence $|\rho_{n_1m}(t)|$ would exhibit the same behavior as that of an effective driven two-level system,

$$\frac{\partial \rho_{n_1m}}{\partial t} \approx -i \frac{\Omega_1^* \Omega_2}{\Delta_1} (\rho_{n_1n_1} - \rho_{mm}), \quad (24)$$

with the Rabi oscillation being governed by vibrational two-photon Rabi coupling $\Omega_1^* \Omega_2/\Delta_1 = \Omega_{2\text{ph}}^v$. Note that the evolution of $\rho_{n_1m}(t)$ would thus become independent of the evolution of the state $|n_2\rangle$, as it would appear in long-pulse-duration couplings. However, in the case of fs laser coupling, the *rotational couplings will inevitably be present*. (3) From Eqs. (20) and (21), the rotational and vibrational coherence are coupled with a coupling factor $\Omega_{2\text{ph}}^v$. In particular, $\partial \rho_{n_1m}/\partial t \propto -i \Omega_{2\text{ph}}^v \rho_{n_1n_2}$, which explains why the Rabi oscillations appear in $|\rho_{n_1m}(t)|$ in Fig. 3(b), corresponding to the saturation of the rotational coherence even though the maximum value of $|\rho_{n_1m}(t)|$ is still far from the maximum achievable value of 0.5. Physically, this may be understood as follows: The rotational coherence $\rho_{n_1n_2}$ exhibits Rabi oscillation for pump intensities above the saturation threshold, where the rotational populations in $|n_1\rangle$ and $|n_2\rangle$ also oscillate. Such population oscillation is translated into oscillations in the rovibrational coherence ρ_{n_1m} when either of the $|n_i\rangle$ states is coupled to the state $|m\rangle$ via two-photon Raman coupling (pump and Stokes), even though the vibrational coherence is far from its maximum achievable value. (4) Above the saturation threshold, the vibrational-coherence evolution has a very strong dependence on itself, which is scaled by a factor of $\Omega_{2\text{ph}}^R$ [see Eq. (23)]; however, the rotational-coherence evolution is primarily dependent on the population inversion in the rotational states and $\Omega_{2\text{ph}}^R$ [see Eq. (22)]. (5) It is also clear from both Eqs. (20) and (21) that the evolutions of both coherences will always be scaled down by the detuning Δ_1 . We now examine the effect of wavelength shifts of the pump and Stokes pulses (especially toward the blue region) on the saturation of rotational and vibrational coherences.

Next, returning to the full numerical solutions of the coupled density-matrix equations (9)–(17), in Fig. 4(a) we have plotted the magnitude of the rotational coherence $|\rho_{n_1n_2}|$ at $t = 2.5$ ps as a function of pump intensity for a different pair of pump and Stokes wavelengths λ_1 and λ_2 , respectively, in such a way that the Raman resonance is maintained but the detuning of the central frequency of the pump Δ_1 from the electronic transition differs by a factor of ~ 2.5 . All other parameters are maintained at the same values as in Fig. 3. It is clear that for $\lambda_1 = 675$ nm and $\lambda_2 = 800$ nm, the coherence has a linear dependence until the pump intensity reaches

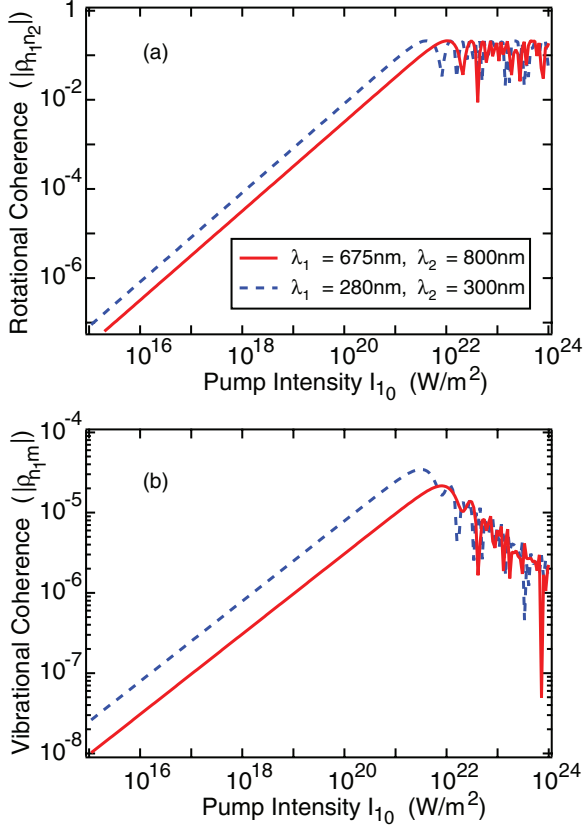


FIG. 4. (Color online) (a) Saturation of rotational coherence as a function of the peak intensity of the pump. The two saturation curves correspond to different single-photon detunings Δ_1 for a pair of Raman-resonant pump and Stokes pulses. (b) The saturation in vibrational coherence corresponds to the same conditions as in (a).

$I_1 \sim 10^{22}$ W/m²; then the coherence value saturates. Using bluer pump and Stokes pulses (red dashed lines), the saturation threshold is reduced by almost one-half. The corresponding vibrational coherence $|\rho_{n_1 m}|$ is plotted in Fig. 4(b). Once again, the saturation threshold of the vibrational coherence exhibits behavior similar to that for the rotational coherence for bluer pump and Stokes pulses. The magnitude of $|\rho_{n_1 m}|$ above the saturation threshold is reduced drastically with increasing I_1 , unlike that of $|\rho_{n_1 n_2}|$. This may be explained by the third note after Eq. (23). However, since, within the framework of four-wave mixing, the effects of all orders are included in the numerical calculations presented here, the role of many other possible high-order nonlinear effects cannot be ruled out.

B. Saturation of the CARS signal

In this section we present numerical results showing how the CARS signal is affected when a time-delayed fs probe pulse scatters off the vibrational coherence, which is generated by a parametrically varying pump intensity—in particular, what happens when the coherence saturates. Once again, since the focus is on the effect of saturation of the rotational coherence on the CARS signal, we parametrically change the peak intensity of the pump and calculate I_{CARS} using Eq. (19). All of the parameters used in this numerical study are the same as those in Fig. 3; in addition, the peak intensity of the

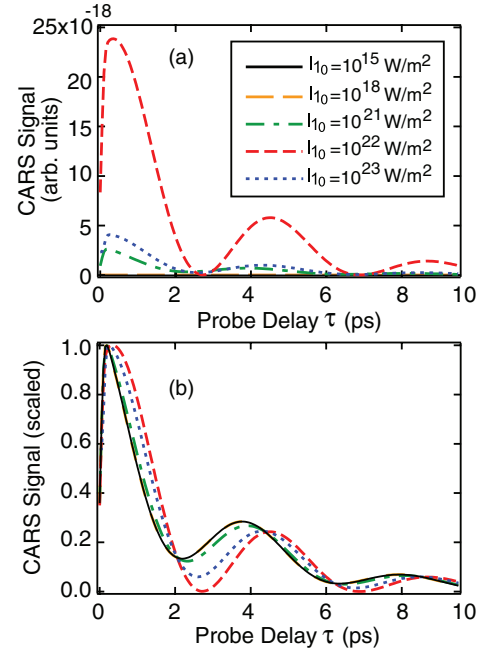


FIG. 5. (Color online) (a) Saturation of the CARS signal (in arbitrary units) as a function of probe delay. (b) Scaled CARS signal where the peaks shift, which could be because of a Stark shift of the rotational states.

probe is $I_3 \sim 10^{15}$ W/m², with its central frequency centered at 800 nm and a pulse duration of $\tau_3 = 100$ fs. The probe is delayed by τ , as shown in Fig. 5. In Fig. 5(a), the CARS signal is plotted as a function of the probe delay for peak intensities of the pump starting at $I_1 = 10^{15}$ W/m² and increasing until they are above the saturation threshold of $I_1 > 10^{22}$ W/m². As expected, once the rotational coherence $|\rho_{n_1 n_2}|$ crosses the saturation threshold, the vibrational coherence also decreases in the same conditions; effectively the probe scatters off a weaker rovibrational coherence beyond the threshold pump intensity and, hence, the CARS signal decreases [shown as blue dotted lines in Fig. 5(a)]. It should also be noted that here the rovibrational CARS signal exhibits oscillations unlike those in the experimental room-temperature N₂ CARS signal, because in our model we have limited ourselves to only two rotational states in the ground vibrational levels, and the oscillation is reminiscent of the beating between the two rotational Raman lines. Such beatings are prevalent in other fs CARS studies where only a few states are involved in the interaction [34]. In Fig. 5(b) we replot the CARS-signal data in Fig. 5(a), with their values scaled to unity. A few important observations should be noted from this figure: For a peak intensity well below the saturation intensity $I_{10} < 10^{22}$ W/m², the oscillations in the CARS signal are very close to those in the linear regime (solid black line). However, for peak intensities closer to and above saturation, the slopes of the curves change and the peaks shift toward a longer probe delay. Thus, the oscillation frequencies and also the depth of the oscillations have changed. This clearly indicates a possible Stark shift of the rotational states by the intense pump field at peak intensities of $I_{10} > 10^{22}$ W/m². Therefore, the rotational saturation may distort the spectral signature as a result of such shifts.

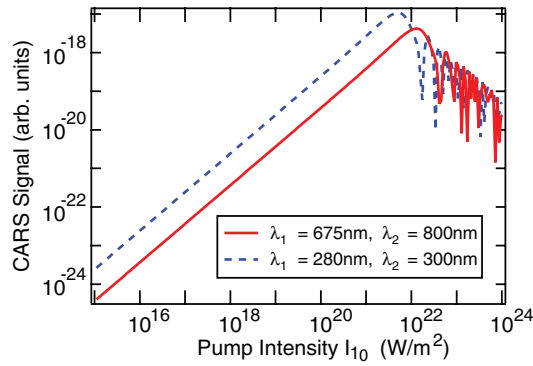


FIG. 6. (Color online) Saturation of CARS signal (in arbitrary units) as a function of peak intensity of the pump for two pairs of pump and Stokes fields.

We also examine the saturation threshold of the CARS signal when we use bluer pump and Stokes pulses. In Fig. 6, we plot the maximum CARS signal for the same two pairs of pump and Stokes pulses as those used in Fig. 4. The probe delay is considered to be 2 ps. The CARS signal exhibits characteristic saturation similar to that of the rovibrational coherence presented in Fig. 4(b)—the saturation threshold for the CARS signal decreases with bluer pump and Stokes pulses. Also the CARS signal is reduced by a few orders of magnitude if the peak intensity of the pump is increased beyond the saturation limit. It should also be noted that the CARS signal obtained is consistently higher for bluer pump and Stokes pulses for each of the peak intensities of the pump because the single-photon detunings are smaller and, hence, the Raman coupling is stronger.

IV. COMPARISON OF VARIOUS THRESHOLDS AND DISCUSSION

Saturation of the Raman transition in the fs regime has been discussed briefly by Lucht *et al.*, who studied the combined effect of the product of the peak intensities of the pump and Stokes pulses on the vibrational-coherence matrix elements and populations and also on the CARS signal [29]. They reported that, for a condition similar to ours, the calculated Raman coherence saturated when the product of the peak powers of the pump and Stokes pulses ($I_1 I_2$) was greater than $5 \times 10^{35} \text{ W/m}^2$. However, they did not study the effect of saturation of the rotational coherence on the vibrational coherence—and, hence, the CARS signal.

In the following we present a discussion on the comparison of our result with those in different nonlinear threshold regimes and also with other pulse-duration excitation regimes.

(a) *Comparison with the threshold of filament formation.* The intensity threshold for Raman saturation determined from our current model study is $\sim 10^{22} \text{ W/m}^2$. However, from a detailed study as noted below, the onset of various other nonlinear processes is inevitable before the threshold for Raman saturation can be achieved. In recent years extensive studies have shown that propagation of an intense short pulse through the air is governed by two competing processes: (1) the natural diffraction of the beam due to the

$\chi^{(3)}$ -modified refractive index causes self-focusing [35] and (2) the defocusing caused by the plasma formed at the focusing volume leads to formation of filaments along the direction of propagation of the pulse [36]. Mourou and co-workers first demonstrated that a 200-fs laser pulse with 50 mJ/pulse operating at 775 nm exhibited filaments in air, and their peak-intensity estimate inside the filaments was $\sim 10^{18} \text{ W/m}^2$ [37]. Hence, no matter how high the peak power of the laser and how tight the laser focus, the peak intensity is clamped at $\sim 10^{18} \text{ W/m}^2$ [38]. Thus, *Raman saturation of N_2 (or air) may not be achievable with fs excitation at room temperature and atmospheric pressure.* However, in higher-pressure gases [39] or in dense condensed-phase systems [40], the Raman-saturation threshold is expected to decrease. The higher threshold of Raman saturation as compared to that of the other nonlinear processes may be due to the reduced coupling efficiency that results from the absence of resonant or near-resonant electronic couplings. The Raman-saturation threshold is also expected to be reduced by at least a few orders of magnitude if electronic-resonant pump and Stokes pulses are used, which will be discussed elsewhere.

(b) *Comparison with air-breakdown thresholds (ns and fs regimes).* Next, we discuss the nonlinear thresholds for the laser powers and intensities in different pulse-duration regimes. A ns laser beam with intensity slightly above the Raman saturation ($> 10^{14} \text{ W/m}^2$) causes air breakdown (0.1% of the molecular gas ionizes in the focal volume) when propagating through air [41]. Thus, a typical laser beam with a 10-ns pulse duration and 50-mJ energy that is focused down to $\sim 50\text{-}\mu\text{m}$ beam waist having a modest peak intensity of $\sim 10^{15} \text{ W/m}^2$ (compared to the peak intensities of the fs pulses) breaks down air and produces air plasma. However, in a regular fs CARS experiment, the most intense beam (the Stokes beam) is typically a 100-fs, 25- μJ pulse with the beam focused to 100- μm diameter, which produces a peak intensity of $2 \times 10^{16} \text{ W/m}^2$. This is at least an order of magnitude higher than the peak breakdown-threshold intensity in the ns regime; however, air breakdown does not occur. The physics of air breakdown in different pulse-duration regimes can be understood as follows. For ns-pulse propagation, the air breakdown process involves three steps: (1) weak multiphoton ionization of impurities in the gas that works as a seeding process for the next two steps, (2) inverse bremsstrahlung where the seed electrons are accelerated in the electromagnetic field of the laser, and (3) avalanche ionization, where the accelerated electrons collide with other molecules to produce massive ionization and, hence, plasma in air [42]. Thus, unlike in fs laser propagation, once the ns laser peak power approaches the critical power for self-focusing [43], the above three-step process results in gas breakdown. Note that the latter two processes are collisional in nature and that their time scale of action is between ns and ps. Therefore, with fs excitation (up to 100 fs), the pulse duration is insufficient to initiate even a single inverse-bremsstrahlung process; thus, even at a critical power of the laser which is higher than that required for self-focusing, avalanche ionization never occurs [36]. However, at higher intensities multiphoton ionization can occur to produce underdense plasma, but the ion density will be clamped because of intensity clamping [44]. In a recent report, it was shown that laser-induced breakdown

can be achieved because of multiphoton ionization only, and a possible realization of partial avalanche breakdown is demonstrated using high-repetition-rate (1-kHz) pulses in noble gases [45]. Thus, in fs excitation, a much higher-intensity pump can propagate through air without breakdown than in the case of the ns lasers. But, once again, since the air-breakdown threshold intensity in the fs-pulse-duration regime is smaller than that for Raman saturation calculated in ambient air, Raman saturation of N_2 (or air) may not be achievable.

(c) *Comparison with the ns Raman-saturation threshold.* Comparison of the Raman saturation obtained in the current study with that of longer-pulse-duration regimes leads to interesting observations. For ns excitations, since the bandwidth of the pulse is sufficient to excite only one Raman line at a time, simultaneous rotational coupling cannot occur. However, we can still compare the Raman-saturation thresholds in different pulse-duration regimes to aid the understanding of the fundamental differences in their origins. In ns CARS of N_2 , it has been reported that the peak intensity of a 20-ns pump required to observe the Stark shift is on the order of $\sim 10^{14}$ W/m² [4]. For fs excitation, the peak intensity required for saturation is at least six to seven orders of magnitude higher than that for ns excitation. This huge discrepancy in saturation thresholds can be understood as follows: In the cw or long-pulse regime, the saturation of Raman coherence occurs if the two-photon Rabi frequency (in an effective two-level model [46])

$$\Omega_{2\text{ph}} = \frac{\Omega_1 \Omega_2}{\Delta_1} \quad (25)$$

can overcome all of the decay and dephasing rates of the rovibrational levels—usually $\Omega_{2\text{ph}} > \sqrt{\gamma_i \Gamma_j}$. With short pulses of fs duration that have very high peak powers but are short lived, the molecular response time would also become important in determining the saturation thresholds, which is the subject of the current discussion. In fact, recently it has been shown in a two-photon fluorescence experiment with fs excitation that the Rabi flopping of a transition depends linearly on the pulse area [47]. For our off-resonant Raman system, the total two-photon pulse area can be calculated in real time as

$$\Theta_{2\text{ph}}(t) = \frac{1}{\Delta_1} \int_{-\infty}^t \Omega_1(t') \Omega_2(t') dt'. \quad (26)$$

For saturation to occur, the total pulse area $\Theta_{2\text{ph}}(t \rightarrow \infty)$ should be at least a few π ; physically, at least a few Rabi cycles of population should occur between the transitions of interest before they can be saturated. Therefore, two ways in which one can achieve large pulse areas in our model are (1) by increasing the peak intensities of the pump I_{10} and Stokes I_{20} pulses or (2) by increasing the pulse duration. For ns CARS and even ps CARS, the pulse-area condition is easily met, whereas, for fs excitation of the N_2 molecule, the pulse durations τ_1 and τ_2 are so short that to observe any significant Rabi oscillation in rotational coherence requires the peak intensity of the pump $I_1 > 10^{22}$ W/m² (as shown in Fig. 3)—which, of course, is translated into oscillations in populations (not shown here). For a proof-of-principle test of the role of the pulse duration τ_i in the saturation threshold, we have plotted

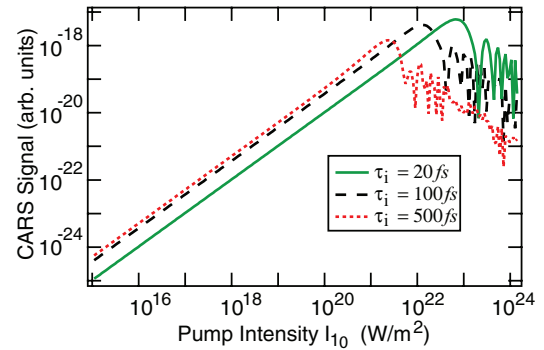


FIG. 7. (Color online) Saturation of CARS signal as a function of peak intensity of the pump for pulse durations of 20 fs (solid line), 100 fs (dashed line), and 500 fs (dotted line).

the CARS signal obtained from the numerical solutions of the density-matrix equations (9)–(17) as a function of peak intensity of the pump field for different τ_i in Fig. 7. All of the parameters considered here are the same as those of the red solid curve in Fig. 6, except for the changing durations of the pulses $\tau_i \sim 20, 100,$ and 500 fs and the corresponding probe delays of $\sim 20\tau_i$. It is clear that the threshold of saturation is decreased by almost an order of magnitude with a five-times increase in the pulse duration of the Raman excitation pulses. The rotational and vibrational coherences for different τ_i exhibit the same behavior (not presented here). This result is in accordance with the discussion following Eq. (26). We assume that such a decline in saturation threshold will continue to the long-pulse regime perhaps up to the ns regime, but we cannot quantitatively generalize the rate of decline in the saturation threshold. The primary reason is that the major difference in the saturation threshold would arise from the rotational couplings due to the bandwidths associated with the excitation pulses. Thus, a model that includes additional rotational states would provide a more complete picture; this work is in progress. Equation (26) also indicates a third possibility for increasing the pulse area by decreasing Δ_1 , which implies Raman excitations by electronic-resonant or near-electronic-resonant pump and Stokes pulses [48]—a subject that will be discussed elsewhere.

V. SUMMARY

We have studied fs CARS using a model four-level system; we have specifically investigated the effect of simultaneous coupling of multiple rotational states by the broad bandwidth associated with a fs pump on the saturation of Raman coherences and rovibrational CARS. We have demonstrated that the saturation of rotational coherence occurs after it reaches its near-maximum value, whereas the saturation of vibrational coherence occurs when its magnitude is still far from the maximum achievable value. Bluer pump and Stokes pulses have been shown to lower the threshold of saturation of rotational coherence, vibrational coherence, and CARS; we have shown this both numerically and also with the use of reduced analytical equations. We have compared our results with other fs nonlinear thresholds and found that gas-phase Raman saturation of N_2 with fs pulses in the optical-frequency regime may

never be observed. Also, we have shown that the requirements for saturations differ fundamentally in the ns and fs excitations; we have provided an explanation for the large discrepancy in their saturation thresholds. Preliminary investigations have shown that in the gas phase, the saturation of Raman coherence—and, hence, CARS—using fs excitations may be possible in high-pressure gases or in near-electronic-resonant couplings.

ACKNOWLEDGMENTS

Funding for this study was provided by the US Air Force Research Laboratory (Contracts No. F33615-03-D-2329 and No. FA8650-10-C-2008) and the US Air Force Office of Scientific Research. This manuscript has been cleared for public release (No. 88ABW-2012-6541). The authors would like to thank Dr. Alan Eckbreth for inspiring this work through stimulating discussions.

-
- [1] W. Demtroder, *Laser Spectroscopy* (Springer-Verlag, Berlin/Heidelberg, 2008), Vol. 2.
- [2] A. C. Eckbreth, *Laser Diagnostics for Combustion Temperature and Species* (Gordon and Breach, Amsterdam, 1996).
- [3] L. A. Rahn, R. L. Farrow, M. L. Koszykowski, and P. L. Mattern, *Phys. Rev. Lett.* **45**, 620 (1980).
- [4] R. L. Farrow and R. P. Lucht, *Opt. Lett.* **11**, 374 (1986).
- [5] M. Pealat, M. Lefebvre, J. P. E. Taran, and P. L. Kelley, *Phys. Rev. A* **38**, 1948 (1988).
- [6] R. P. Lucht and R. L. Farrow, *J. Opt. Soc. Am. B* **5**, 1243 (1988).
- [7] G. Magnotti, A. D. Cutler, G. C. Herring, S. A. Tedder, and P. M. Danehy, *J. Raman Spectrosc.* **43**, 611 (2012).
- [8] R. P. Lucht, R. L. Farrow, and D. J. Rakestraw, *J. Opt. Soc. Am. B* **10**, 1508 (1993).
- [9] R. T. Bratfalean, G. M. Lloyd, and P. Ewart, *J. Opt. Soc. Am. B* **16**, 952 (1999).
- [10] T. A. Reichardt, F. D. Teodoro, R. L. Farrow, S. Roy, and R. P. Lucht, *J. Chem. Phys.* **113**, 2263 (2000).
- [11] S. Roy, R. P. Lucht, and T. A. Reichardt, *J. Chem. Phys.* **116**, 571 (2002), and references therein.
- [12] A. K. Patnaik, S. Roy, R. P. Lucht, and J. R. Gord, *J. Mod. Opt.* **55**, 3263 (2008).
- [13] A. K. Patnaik, S. Roy, J. R. Gord, R. P. Lucht, and T. B. Settersten, *J. Chem. Phys.* **130**, 214304 (2009).
- [14] J. P. Kuehner, S. V. Naik, W. D. Kulatilaka, N. Chai, N. M. Laurendeau, R. P. Lucht, M. O. Scully, S. Roy, A. K. Patnaik, and J. R. Gord, *J. Chem. Phys.* **128**, 174308 (2008).
- [15] A. C. Eckbreth and T. J. Anderson, *Appl. Opt.* **24**, 2731 (1985).
- [16] S. Roy, J. R. Gord, and A. K. Patnaik, *Prog. Energy Combust. Sci.* **36**, 280 (2010).
- [17] D. Oron, N. Dudovich, D. Yelin, and Y. Silberberg, *Phys. Rev. Lett.* **88**, 063004 (2002).
- [18] W. D. Kulatilaka, H. U. Stauffer, J. R. Gord, and S. Roy, *Opt. Lett.* **36**, 4182 (2011).
- [19] J. D. Miller, S. Roy, M. N. Slipchenko, J. R. Gord, and T. R. Meyer, *Opt. Express* **19**, 15627 (2011).
- [20] J. D. Miller, S. Roy, J. R. Gord, and T. R. Meyer, *J. Chem. Phys.* **135**, 201104 (2011).
- [21] P. J. Wrzesinski, H. U. Stauffer, S. Roy, and J. R. Gord, *J. Raman Spectrosc.* (to be published).
- [22] S. Roy, P. Wrzesinski, D. Pestov, T. Gunaratne, M. Dantus, and J. R. Gord, *Appl. Phys. Lett.* **95**, 074102 (2009).
- [23] V. Kocharovskiy, S. Cameron, K. Lehmann, R. Lucht, R. Miles, Y. Rostovtsev, W. Warren, G. R. Welch, and M. O. Scully, *Proc. Natl. Acad. Sci. USA* **102**, 7806 (2005).
- [24] J. R. Gord, T. R. Meyer, and S. Roy, *Annu. Rev. Anal. Chem.* **1**, 663 (2008).
- [25] M. O. Scully and M. S. Zubairy, *Quantum Optics* (Cambridge University Press, Cambridge, 1997).
- [26] D. A. Long, *The Raman Effect* (John Wiley and Sons, Chichester, West Sussex, 2002).
- [27] D. E. Shemansky and N. P. Carleton, *J. Chem. Phys.* **51**, 682 (1969).
- [28] F. R. Gilmore, R. R. Laher, and P. J. Espy, *J. Phys. Chem. Ref. Data* **21**, 1005 (1992).
- [29] R. P. Lucht, P. J. Kinnius, S. Roy, and J. R. Gord, *J. Chem. Phys.* **127**, 044316 (2007).
- [30] T. Ahn, I. V. Adamovich, and W. R. Lempert, *Chem. Phys.* **298**, 233 (2004).
- [31] L. A. Rahn and R. E. Palmer, *J. Opt. Soc. Am. B* **3**, 1164 (1986).
- [32] N. Owschimikow, F. Konigsmann, J. Maurer, P. Giese, A. Ott, B. Schmidt, and N. Schwentner, *J. Chem. Phys.* **133**, 044311 (2010).
- [33] R. P. Lucht, S. Roy, T. R. Meyer, and J. R. Gord, *Appl. Phys. Lett.* **89**, 251112 (2006).
- [34] T. Lang and M. Motzkus, *J. Raman Spectrosc.* **31**, 65 (2000).
- [35] Y. R. Shen, in *Self-Focusing and Filaments of Light: Past and Present*, edited by R. W. Boyd, S. G. Lukishova, and Y. R. Shen (Springer, New York, 2009), Vol. 114, p. 3.
- [36] For an excellent review on ultrashort laser propagation and filamentation, see S. L. Chin, T. J. Wang, C. Marceau, J. Wu, J. S. Liu, O. Kosareva, N. Panov, Y. P. Chen, J. F. Daigle, S. Yuan, A. Azarm, W. W. Liu, T. Seideman, H. P. Zeng, M. Richardson, R. Li, and Z. Z. Xu, *Laser Phys.* **22**, 1 (2011).
- [37] A. Braun, G. Korn, X. Liu, D. Du, J. Squier, and G. Mourou, *Opt. Lett.* **20**, 73 (1995).
- [38] A. Becker, N. Akozbek, K. Vijayalakshmi, E. Oral, C. M. Bowden, and S. L. Chin, *Appl. Phys. B: Lasers Opt.* **73**, 287 (2001).
- [39] C. L. M. Ireland and C. G. Morgan, *J. Phys. D* **6**, 720 (1973).
- [40] E. L. Gurevich and R. Hergenroder, *Appl. Spectrosc.* **61**, 233A (2007).
- [41] R. Meyerand and A. Haught, *Phys. Rev. Lett.* **11**, 401 (1963).
- [42] S. L. Chin, in *Advances in Multiphoton Processes and Spectroscopy*, edited by S. H. Lin, A. A. Villaeys, and Y. Fujimura (World Scientific, Singapore, 2004), Vol. 16, p. 273.
- [43] R. Chiao, E. Garmire, and C. Townes, *Phys. Rev. Lett.* **13**, 479 (1964).
- [44] R. Rankin, E. E. Capjack, N. H. Burnett, and P. B. Corkum, *Opt. Lett.* **16**, 835 (1991).
- [45] A. M. Heins and C. Guo, *Opt. Lett.* **37**, 599 (2012).
- [46] A. D. Wilson-Gordon, R. Klimovsky-Barid, and H. Friedmann, *Phys. Rev. A* **25**, 1580 (1982).
- [47] J. Lim, K. Lee, and J. Ahn, *Opt. Lett.* **37**, 3378 (2012).
- [48] L. Yuan, G. O. Ariunbold, R. K. Murawski, D. Pestov, X. Wang, A. K. Patnaik, V. A. Sautenkov, A. V. Sokolov, Y. V. Rostovtsev, and M. O. Scully, *Phys. Rev. A* **81**, 053405 (2010).